Smooth Autonomous Take-off and Landing Maneuvers over a Double-hulled Watercraft

Omar Velasco, Pablo J. Alhama Blanco and João Valente
Departamento de Ingeniería de Sistemas y Automatica, Universidad Carlos III de Madrid, Leganés, Madrid, Spain

Keywords: Aerial-marine Robotic System, Vertical Take-off and Landing, Classic Control, Dynamic Movement Primitives.

Abstract: This paper addresses the problem of vertical take-off and landing (VTOL) over a moving target in an inland water environment. The maneuvers are carried out by a multi-rotor unmanned aerial system (UAS) over a double-hulled watercraft unmanned surface vehicle (USV). The approach proposed employs a cascade PID control architecture and is then improved with Dynamic Movement Primitives (DMP). The results presented show that DMP can be used in combination with PID classical control for achieving a more safe and accurate VTOL maneuver.

1 INTRODUCTION

Quality assessment of inland waters is one of the most important action fields launched by the European Union until 2022 for biodiversity and habitat conservation.

The branch of science that addresses the studies of inland aquatic ecosystems is called limnology. Water quality evaluation is achieved through the analysis and classification of different biophysical and biochemical parameters. This parameters are usually acquired locally with manual instrumentation close by the water, and also through satellites or airborne imagery.

Manual sampling techniques have been used traditionally, but they involve tedious operations and increase the probability of erroneous field practices. Moreover, satellite imagery is not always available and the spatial resolution is limited for certain applications. Finally, airborne surveys are subject to strict legislation for flying over natural environments and ungovernable logistics. It should also be highlighted that all those approaches have increased associated operation costs.

Unmanned aerial systems (UAS) have improved remote sensing (RS) missions from different domains by providing a personal channel of data delivery for researcher and end-users. In this way, their usability in limnology will also play an important role because data may be delivered in short time windows and with affordable operation costs.

The UAS can be successful used in aquatic environments (Ore et al., 2015), however they have a very limited autonomy, and they might be vulnerable to unexpected weather changes. In order to avoid accidents and damages to the platform it is important to constantly have available an emergency landing platform fot the UAS during the mission.

In this paper we present a set of control strategies for autonomous vertical takeoff and landing (VTOL) with a quadrotor and a double-hulled watercraft.

A multiple robot UAS-USV configuration was presented in (Djapic et al., 2015) focusing on the implementation of the control approach and the communication interfaces. In (Pinto et al., 2014) a more complex collaboration system was designed for environmental data gathering with autonomous operation, including VTOL. Another aerial and marine collaboration using a visual servoing algorithm is presented in (Weaver et al.,).

The work presented herein can be distinguished by the smaller scale of the aerial platforms in the multi-robot team. This characteristic enables rapid deployment in areas with difficult access and hard to survey. Moreover, a reliable path tracking controller for smooth landing and take off sequences was designed to minimize the risk of the quadcopter falling into the water during the VTOL manoeuvres.

This paper is organized as follows: The background of the problem is firstly given. Then, the platforms used, as well as the scenario, and the assumptions are introduced in Section 2. Section 3 explains

Velasco, O., Blanco, P. and Valente, J.
Smooth Autonomous Take-off and Landing Maneuvers over a Double-hulled Watercraft.
DOI: 10.5220/0006435303890396
In *Proceedings of the 14th International Conference on Informatics in Control, Automation and Robotics (ICINCO 2017) - Volume 2*, pages 389-396
ISBN: Not Available

how the platforms dynamic models were obtained, followed by the control strategy applied in Section 4. After that, DMPs are presented and used to improve the previous control approach in Section 5. Simulations results are presented in Section 6, and conclusion remarks in Section 7.

2 ROBOTIC SYSTEM, SCENARIO AND ASSUMPTIONS

This section presents the multi-robot team modelled in this work, and covers the characteristics of the modeling scenario.

2.1 Robotic System

The modelled aerial platform is based in the AR.Drone quadcopter, while the USV is a built from the scratch platform named Strider V1.0. The objective of this multi-robot solution is to provide a collaboration system to perform data collection tasks in relatively still waters. The USV aims to provide longer autonomy to the UAV behaving as a mobile landing platform and charging station. The drone provides the agility and flexibility to access zones where the USV cannot reach.

2.2 Scenario and Assumptions

The solution presented in this work is particularly destined to inland water environments where wave incidence is negligible. The assumptions made during the dynamic modeling of both vehicles will be based upon this conditions. Therefore, angle variation in the USV's roll, pitch and heave are not considered.

3 DYNAMIC MODELING

This section deals with the dynamic modeling of the two autonomous vehicles presented in this work. We consider the UAV and the USV as single rigid body systems to obtain the models of their dynamics. The Newton-Euler formalism will be used to describe the motion of both autonomous platforms.

3.1 Quad-rotor Helicopter

Concerning quadcopter modeling, an inertial and a fixed-body frame will be defined, following the notation in Figure 1, where E is the inertial earth frame,

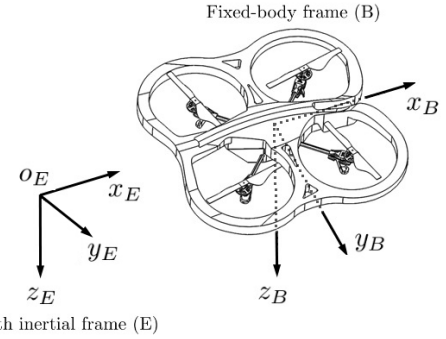

Figure 1: Coordinate system schematic and notation for the quadcopter motion description.

following a right handed NED coordinate system convention, and B is the body-fixed frame, attached to the quadcopter airframe and along the arms of the quadrotor.

Let us then define the following workspace within this two frames. Two vectors can be defined to give a generalized overview of the position and velocity of the quadrotor in the space:

$$\xi = \begin{bmatrix} \Gamma^E & \Theta^E \end{bmatrix}^T = \begin{bmatrix} x_q & y_q & z_q & \phi_q & \theta_q & \psi_q \end{bmatrix}^T \quad (1)$$

$$\nu_q = \begin{bmatrix} \mathbf{V}^B & \omega^B \end{bmatrix}^T = \begin{bmatrix} u_q & v_q & w_q & p_q & q_q & r_q \end{bmatrix}^T \quad (2)$$

Where ξ $[+]$ represents the generalized position of the body with in terms of the earth frame and ν_q $[+]$ the generalized velocity of the quad-copter in terms of the body frame. The vector $\mathbf{V}^B$ $[m\ s^{-1}]$ represents the linear velocity vector of the body frame with respect to the inertial frame, being u_q, v_q and ω_q the velocities in the positive x_B, y_B and z_B directions respectively. Similarly, the vector ω^B $[rad\ s^{-1}]$ represents the angular velocity of the quadrotor with respect to the inertial frame, being p_q, q_q and r_q the angular velocities around the x_B, y_B and z_B axis. Γ^E $[m]$ and Θ^E $[rad]$ represent the linear and angular position, being x_q, y_q and z_q the position of the body frame with respect to the earth frame and ϕ_q stands for roll, θ_q for pitch and ψ_q for yaw of the body frame with respect to the inertial frame.

Before we delve into the expressions for the motion of the quadrotor we will set a series of assumptions in order to simplify this task:

1. The body-fixed frame axes coincide with the principal axes of inertia of the body
2. The moments of inertia are constant.
3. The body-fixed frame origin o_B is coincident with the centre of mass.
4. Body symmetry with respect to the centre of mass is assumed.

5. Minor aerodynamic effects such as blade flapping or induced drag are not considered.

Using the previously defined workspace we can obtain an expression for the motion of the quadcopter. Equation 3 expresses the generalized expression for the motion of any rigid body based on the assumptions made before:

$$\begin{bmatrix} m_q I_{3\times3} & \mathbf{0}_{3\times3} \\ \mathbf{0}_{3\times3} & I \end{bmatrix} \begin{bmatrix} \dot{\mathbf{V}}^B \\ \dot{\omega}^B \end{bmatrix} + \begin{bmatrix} \omega^B \times (m_q \mathbf{V}^B) \\ \omega^B \times (I\omega^B) \end{bmatrix} = \begin{bmatrix} \mathbf{F}^B \\ \tau^B \end{bmatrix} \quad (3)$$

Where m_q $[Kg]$ is the mass and I $[N\ m\ s^2]$ is the inertia matrix of the quadrotor, with respect to the body frame, and $\tau^B[N\ m]$ and $\mathbf{F}^B[N]$ are the force and torque with respect to the body frame. We can characterize this expression to the quadcopter model by defining the force and torque vector at the right side of the equation. In the case of the quadcopter model, this force and torque vector, shown in equation 4, can be divided into four components:

$$\begin{bmatrix} \mathbf{F}^B \\ \tau^B \end{bmatrix} = \begin{bmatrix} \mathbf{F}^B_G \\ \mathbf{0}_{3\times1} \end{bmatrix} + \mathbf{U}^B + \begin{bmatrix} \mathbf{0}_{3\times1} \\ \mathbf{G}^B_a \end{bmatrix} + \mathbf{F}^B_{ext} \quad (4)$$

Gravitational Contribution. This component comes from the effect of gravity on the quadrotor. It can be modelled as:

$$\mathbf{F}^B_G(\Theta) = \mathbf{R}_\Theta^{-1}\mathbf{F}^E_G = \mathbf{R}^T_\Theta \begin{bmatrix} 0 \\ 0 \\ m_q g \end{bmatrix} = \begin{bmatrix} -m_q g s(\theta) \\ m_q g c(\theta) s(\phi) \\ m_q g c(\theta) s(\phi) \end{bmatrix} \quad (5)$$

Where $\mathbf{F}^B_G$ is the force vector due to the gravitational contribution expressed in the body frame and $c_\alpha = cos(\alpha)$, $s_\alpha = sin(\alpha)$.

Input Contribution. From the actuation of the four rotors of the quadcopter. Following the typical description of the four basic basic movements of a quadrotor, namely Throttle (U_1), Roll (U_2), Pitch (U_3) and Yaw (U_4) this contribution can be defined as:

$$\mathbf{U}^B = \begin{bmatrix} 0 \\ 0 \\ U_1 \\ U_2 \\ U_3 \\ U_4 \end{bmatrix} = \begin{bmatrix} 0 \\ 0 \\ -c_T(\Omega_1^2 + \Omega_2^2 + \Omega_3^2 + \Omega_4^2) \\ c_T\ l(\Omega_2^2 - \Omega_4^2) \\ c_T\ l(\Omega_1^2 - \Omega_3^2) \\ c_q(\Omega_2^2 + \Omega_4^2 - \Omega_1^2 - \Omega_3^2) \end{bmatrix} \quad (6)$$

Where T_i and Ω_i are the generated thrust and speeds of each rotor respectively, starting by the rotor located in the x_B axis and counting counter-clockwise, c_T $[N\ s^2]$ and c_q $[N\ m\ s^2]$ are the thrust and drag coefficients and l $[m]$ is the distance between the centre of the quadrotor and the centre of the propeller.

Gyroscopic Effects Due to Propeller Rotation. Due to the interaction between the rotating elements of the quadcopter and the airframe. The expression of this gyroscopic torque is given by the following expression (Erginer and Altug, 2007):

$$G^B_a = \sum_{i=1}^{4} I_p(\omega^B \times e_z)(-1)^{i+1}\Omega_i \qquad \in \mathbb{R}^{3\times1} \quad (7)$$

Where I_p $[N\ m\ s^2]$ is the moment of inertia of the propeller, e_z is a unitary vector in the z_E direction and Ω_i the speed of each rotor.

External and Other Forces. Comprising exogenous forces to the quadcopter and other effects, such as minor aerodynamic forces.

3.2 Double-hulled Watercraft

For the dynamic modeling of the Strider V1.0 a similar rigid-body mechanical model to the one used in the previous section is adopted. An inertial and a body fixed frame will be defined to create a suitable workspace for the model. The SNAME (Society of Naval Architects and Marine Engineers) provides with a standard notation and sign convention for the description of the motion of ships shown in Figure 2.

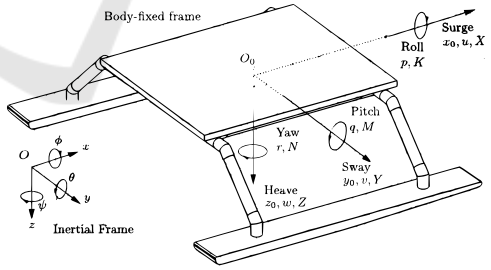

Figure 2: Standard notation and sign conventions for ship motion description on the Strider V1.0.

Again, an inertial earth frame, following the NED convention, and a body-fixed frame, attached to the vehicle's platform, are defined following the notation shown in Figure 2. With this in mind the following notation will be used:

$$\eta^E = \begin{bmatrix} x & y & z & \phi & \theta & \psi \end{bmatrix}^T \quad (8)$$

$$\nu^B = \begin{bmatrix} u & v & w & p & q & r \end{bmatrix}^T \quad (9)$$

$$\Lambda^B = \begin{bmatrix} X & Y & Z & K & M & N \end{bmatrix}^T \quad (10)$$

Where $\eta^E[+]$ is the linear and angular position with respect to the inertial frame, $\nu^B[+]$ the linear and angular velocity of the vessel with respect to the body frame and $\Lambda^B[+]$ represents the forces and torques applied to the vessel in terms of the body fixed frame.

In this work Manoeuvring Theory is adopted to model our simulation. Manoeuvring Theory involves the study of the vessel's movement at a constant or slowly varying positive speed. A three degrees of freedom approach is commonly considered, where only surge, sway and yaw are analysed since restricted, calm water and still waves are assumed (Fossen, 2011). The modelling approach selected in this work, based on a three degrees of freedom (DOF) manoeuvring theory, involves a set of assumptions, summarized in the following list:

1. The body-fixed frame axes coincide with the principal axes of inertia of the body
2. The moments of inertia are constant.
3. Body symmetry with respect to the centre of mass is assumed.
4. The body-fixed frame origin O_0 is coincident with the centre of mass.
5. Restricted, calm and still water bodies is assumed. This implies that no currents or waves affect the motion of the ship.
6. Heave, roll and pitch motions are neglected due to a zero frequency wave excitation assumption.
7. Surge motion is decoupled from sway and yaw motion due to the symmetry of the vessel hulls.
8. Added mass effects on the hulls are neglected since only steady motion will be considered.

Now, taking from the generalized expression for the motion of a rigid body in equation 3, still valid to the model of the Strider V1.0 due to the made assumptions, we can define this 3DOF motion as:

$$\begin{bmatrix} m_v & 0 & 0 \\ 0 & m_v & 0 \\ 0 & 0 & I_z \end{bmatrix} \begin{bmatrix} \dot{u} \\ \dot{v} \\ \dot{r} \end{bmatrix} + \begin{bmatrix} 0 & -m_v r & 0 \\ m_v r & 0 & 0 \\ 0 & 0 & 0 \end{bmatrix} \begin{bmatrix} u \\ v \\ r \end{bmatrix} = \begin{bmatrix} X \\ Y \\ N \end{bmatrix} \quad (11)$$

Where m_v $[Kg]$ is the mass of the vessel. We can characterize this expression to the Strider V1.0 model by defining the forces and torques at play in the motion of the vessel. In the case of the Strider V1.0 model, this force and torque vector can be divided into three components:

Hydrodynamic Effects. This contribution comes from the physical interaction of the hulls with the water. The analytical expression for the hydrodynamic forces is expressed in terms of the hydrodynamic coefficients. In this work the modelling approach made by Davidson and Schiff will be used (Davidson and Schiff, 1946):

$$Y = Y_v v + Y_r r + Y_\delta \delta_R \quad (12)$$

$$N = N_v v + N_r r + N_\delta \delta_R \quad (13)$$

$$X = X(u) + T \quad (14)$$

Where, the constant coefficients ($Y_v = \frac{\partial Y}{\partial v}$ $Y_r = \frac{\partial Y}{\partial r}$ $\cdots$) represent the hydrodynamic derivatives, $X(u)$ is the hydrodynamic resistance (which is a function of the forward speed) and T is the thrust generated by the propeller.

Control Surfaces and Propulsion. Generated by the control surfaces (rudder, fins, etc) and the propulsion forces from the vessel thruster. The propeller thrust is modelled directly as a force, but rudder forces are analytically implemented through the below expression (Perez and Blanke, 2002):

$$\begin{aligned} X_{rudder} &= -F_R(u, V_{av}, v, r, \delta) sin(\delta) \\ Y_{rudder} &= F_R(u, V_{av}, v, r, \delta) cos(\delta) \\ Z_{rudder} &= 0 \end{aligned} \quad (15)$$

Where F_R is defined as:

$$F_R = \begin{cases} \frac{1}{2}\rho C_L A_r V_{av}^2 sin(\frac{\pi}{2}\frac{\delta_{attack}}{\delta_{stall}}) & if |\delta_{attack}| < \delta_{stall} \\ \frac{1}{2}\rho C_L A_r V_{av}^2 sign(\delta_{attack}) & if |\delta_{attack}| \geqslant \delta_{stall} \end{cases} \quad (16)$$

Where ρ $[Kg\ m^-3]$ is the density of the water, C_L $[-]$ is the lift coefficient of the rudder, A_r $[m^2]$ is the rudder area, V_{av} $[m\ s^{-2}]$ is the average flow passing the rudder and δ_{stall} $[rad]$ is the stall angle of the rudder. The function *sign(k)* gives back the sign of k. The angle of attack δ_{attack} $[rad]$ is the angle between the plane of the rudder and the direction of the flow passing by the rudder.

External Forces. Comprising exogenous forces to the vessel such as wind or currents or any other external disturbance.

4 PID CONTROL

PID control techniques are the most used linear regulators. This is due to their simple structure and easy

implementation, good applicability to a wide arrange of control problems and their tunability of "blackbox" systems, where the plant is not identified.

In the case of the quadrotor control system, a PID cascade architecture has been used to obtain control of the vehicle. Figure 3 illustrates the control architecture used in this work for the quadcopter. The implemented architecture features three nested PID feedback loops, each one controlling the position, velocity and attitude of the quadcopter respectively.

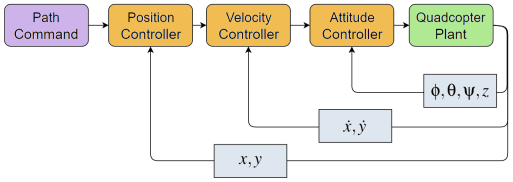

Figure 3: Cascade loop architecture used for the control of the quadcopter.

The control architecture of the Strider V1.0 is easier to implement than the quadrotor system since only two degrees of freedom of the vessel will be controlled. Two separate closed loop PID controllers will command the surge speed u and the heading ψ of the vessel through the actuation of the propeller's thrust and the rudder action respectively.

4.1 Trajectory Tracking

A trajectory tracking algorithm was also implemented in the control architecture of the USV in order to perform planned sweeps and other autonomous path following tasks. Planned routes of any unmanned vehicle can be represented in terms of way-points. Way-points are defined in Cartesian coordinates (x_k, y_k, z_k) for $k = 1, 2, \ldots, n$. and represent an ordered database of points in the working space (Fossen, 2011):

$$wpt.pos = (x_0, y_0, z_0), (x_1, y_1, z_1), \ldots, (x_n, y_n, z_n) \quad (17)$$

One of the simplest and common methods of implementing path control based on way-point trajectory planing is the use of Line Of Sight(LOS) guidance. LOS guidance is based on the calculation of a straight trajectory from the current position of the vehicle and the following way-point using the following expression:

$$\psi_q(t) = tan^{-1}\left(\frac{y_q(k) - y(t)}{x_q(k) - x(t)}\right) \quad (18)$$

Where $\psi_q(t)$ is the desired course angle, $y_q(k)$ and $x_q(k)$ are the next way-point coordinates and $y(t)$ and $x(t)$ the current vehicle position. Once the vehicle has reached the way-point the next way-point is selected. For this purpose, the concept of circle of acceptance is adopted. When the vehicle resides within the borders of a circle of radius ρ_0 $[m]$ the next way-point in the database is selected. This condition is translated into the following inequality:

$$[x_q(k) - x(t)]^2 + [y_q(k) - y(t)]^2 \leq \rho_0^2 \quad (19)$$

4.2 Vertical Take-off and Landing

Autonomous landing on a mobile platform proves to be a difficult task because of the involved complexity of precise position estimation. The usual approach to this problem is the use of Visual Servoing for position and tracking control as works such as (Herissé et al., 2012) show. Although a Visual Servoing servoing algorithm is out of the scope of this work, the performance of VTOL tasks with the designed controller can be evaluated.

The design of the autonomous landing controller is based on the simple flow chart shown in Figure 4. During the approaching phase, the quadrotor is set to track the vessel at an altitude z^* over the landing platform. If the position error e is less than the selected threshold e^*, the quadrotor is commanded to land.

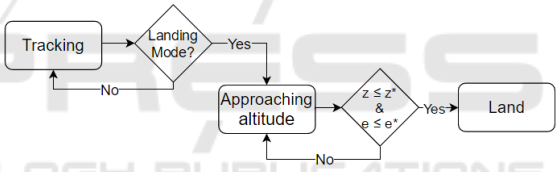

Figure 4: VTOL controller flowchart.

5 DYNAMIC MOVEMENT PRIMITIVES (DMP)

The DMPs have been chosen for improving the VTOL maneuvers because of their ability to operate with all robot control parameters. They are based on nonlinear differential equations. They also provide smooth kinematic control parameters. This is essential to perform all the movements required in a robust and autonomous way. DMPs are well suited to manage uncertainties, uncertain situations, unforeseen events, unexpected events, etc. This is possible for several reasons, first ensuring a smooth transition from any unforeseen changes in the path target due to sensory feedback; Second, because they provide the framework for learning and adapting trajectories using learning and reinforcement algorithms; Thirdly, to allow the learning of all types of trajectories based on one or more of a given trajectory; and lastly because they do not explicitly depend on time.

5.1 Control Parameters as Dynamic Systems

In this section is presented the theoretical foundations of the motor representation developed according to (Ijspeert et al., 2003) and (Schaal et al., 2005). This documents deals with the discrete DMPs that encode discrete point-to-point motion control parameters. For rhythmic DMPs, (Ijspeert et al., 2003) and (Gams et al., 2009) can be consulted. A DMP path with one degree of freedom is defined by (Ijspeert et al., 2013) with the following nonlinear differential equations:

$$\tau \dot{z}_D = \alpha_{z_D}(\beta_{z_D}(g - y_D) - z_D) + f(x_D), \quad (20)$$

$$\tau \dot{y}_D = z_D, \quad (21)$$

$$\tau \dot{x}_D = -\alpha_{x_D} x_D, \quad (22)$$

Where: x_D is the phase variable and z_D is an auxiliary variable that represents the velocity, its derivative is $\dot{z}_D$. Moreover, β_{z_D} , α_{z_D} and α_{x_D} are damping constants, where $\alpha_{z_D} = 4\beta_{z_D}$. The $\tau > 0$ is constant, as a temporal scaling factor. Their values are determined in order to ensure the convergence of the system dynamics. This set of differential equations has a unique attractor point $y_D = g$ (goal) with $z_D = 0$. Finally, $f(x_D)$ is defined as a linear combination of nonlinear radial basis functions, which allow the robot to follow a smooth path from the initial position y_{D0}, to the final configuration g.

$$f(x_D) = \frac{\sum_{i=1}^{M} w_i \Psi_i(x_D)}{\sum_{i=1}^{M} \Psi_i(x_D)} x_D(g - y_{D0}), \quad (23)$$

$$\Psi_i(x_D) = \exp(-h_i(x_D - c_i)^2), \quad (24)$$

Where c_i is the center of the Gaussian distribution along the path phase and h_i is its width. For a given M and considering the time constant $\tau = \tau_T$ can be defined $c_i = \exp(-\alpha_{x_D}\frac{i-1}{M-1})$, $h_i = \frac{1}{(c_{i+1}-c_i)^2}$, $h_M = h_{M-1}$, $i = 0,\ldots,M$. For each degree of freedom in the cartesian space, the weight w_i is estimated by the measured data and using a regression according to (Nemec et al., 2009), g being he last configuration saved during the trajectory. In this way the desired trajectory is obtained. Since discrete DMPs have been designed to represent discrete point-to-point movements, the motion must pass smoothly and continuously at the end of the path, that is, at time τ_T.

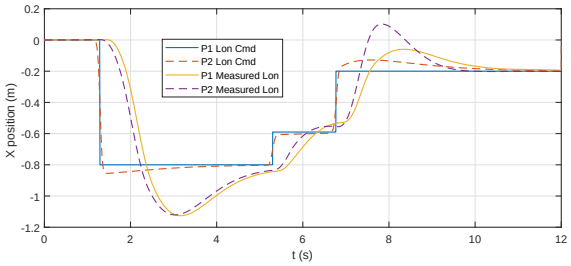

Figure 5: Longitude commands and measured values during the test.

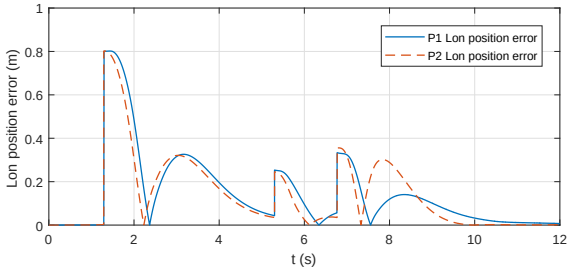

Figure 6: Longitude position errors during the test.

6 EXPERIMENTS

This section will present the results obtained from the simulation of several tests to evaluate the performance of the designed controller.

6.1 Way-point Guidance Test

Way-point guidance was implemented for position control of the Strider V1.0. Several tests were performed with different path setups. Starting from the coordinates origin, a constant speed of 1 m/s was commanded to the vessel since this is the reference speed used for the dynamic modeling of the forces. Further analysis and results of the performance of this controller can be found in (Omar, 2017).

6.2 DMP in Path Tracking Controllers

In this part, the performance of the proposed method of improving a classic control with dynamic movement primitives is evaluated. The base of experiments is centered on three scenarios. A first base scenario P1 in which a control based on a cascade PID control architecture is performed. A second scenario P2 in which changes are introduced by the use of DMPs. Finally a third scenario P3, where it is compared with the case in which the operator handles the quadcopter manually. One of the characteristics of the DMP is the smoothness in the reproduction of movements. For a smooth movement during the course of the tra-

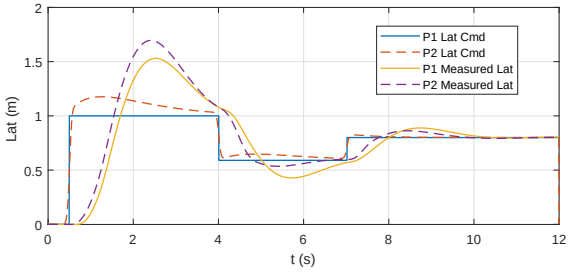

Figure 7: Latitude commands and measured values during the test.

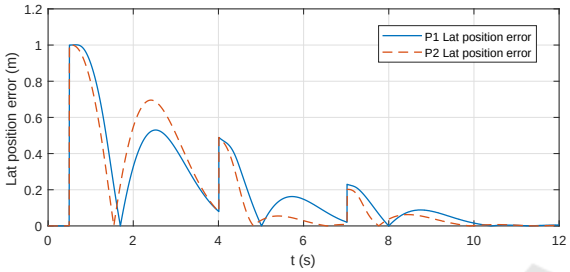

Figure 8: Latitude position errors during the test.

jectory, a treatment of the Cartesian control parameters is carried out using the UAV dynamic model. Within the analyzed parameters we can highlight the VTOL performance of the scenarios P1 and P2. Concerning the path tracking performance, Figures 7 and 5 illustrate the system's path tracking response during tests P1 and P2. The position errors of the quadrotor during flight are shown in 8 and 6. These errors represent the distance between the original position command (that of P1) and the measured latitude and longitude during both tests. Another parameter analyzed is the settling time of the controller. As it can be seen from the results in the figures, especially from the analysis of the error plots, the results from P2 show a quicker settling time, which overall results in a smaller average position error during the test. This behavior, although more aggressive than P1 in some cases (where the error from P2 is bigger than the error from P1) provides a more tight path following performance, which heavily benefits autonomous take off and landing duties. Regarding the behavior against overshoots, it is where more significant improvements are obtained, In figure 9 it is possible to see in a dynamic way the abrupt changes made by the operator of the scenario P3. In front of a soft control parameters thanks to the DMP. Despite of being a very incipient experimentation it can be said that the preliminary results are satisfactory. It is intended to continue to introduce characteristics of the DMP, such as the treatment of rhythmic movements in surveying duties (a typical task for drones) or dynamic evasion of obstacles during VTOL.

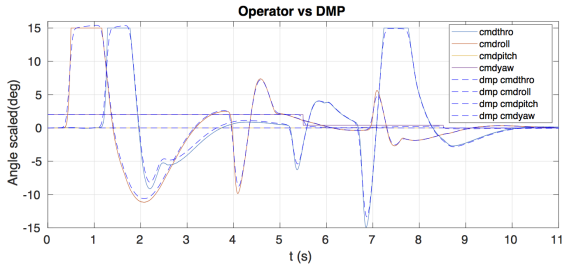

Figure 9: Comparative between operator and DMPs.

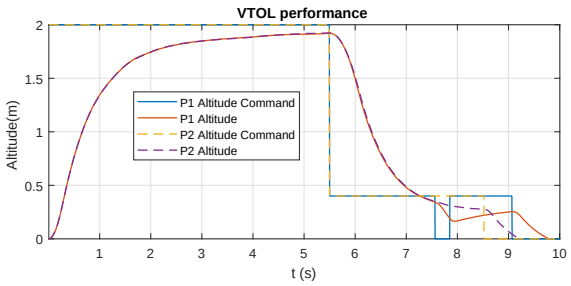

Figure 10: Height values during P1 and P2 testing.

6.3 DMPs and VTOL Tests

We will evaluate the performance of the VTOL and tracking algorithm comparing the two scenarios P1 and P2. The quadrotor is set to track the position of the moving landing platform. It autonomously takes off at the start of the test ($t = 0s$) and then the VTOL controller is activated at 5,5 seconds and set to landing mode. The controller parameters, from Figure 4, used for the test were $e^* = 0.12\ m$ and $h^* = 0.3\ m$.

Figure 10 shows the height measured values and command of the quadrotor during tests P1 and P2. The three phases of the algorithm can be easily identified by seeing the commanded height values during the test, where the three height command levels represent each of the states of the controller respectively. Figure 11 presents the absolute position error, representing the distance from the quadrotor to the centre of the landing pad. As it can be seen from both figures, the performance of the DMP path tracking (P2) yields a much smoother landing sequence. This is thanks to the benefits of the DMP, since the absolute error gets reduced into the minimum landing error threshold.

It can be seen that the VTOL algorithm functions properly and that the quadcopter is able to safely land in the platform within the error constrains that were set in both tests, however when treating the path tracking controller with DMP the results provide with lower landing times, reducing the inherent possibility of hazard during this complicated manoeuvre, and a more fluid landing behaviour.

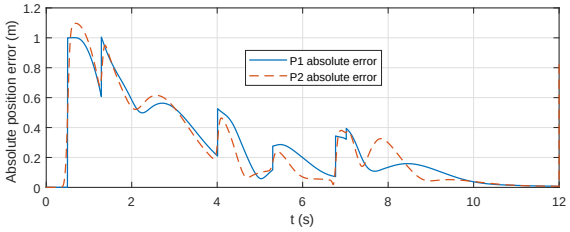

Figure 11: Absolute position error of the quadcopter during the VTOL test.

7 CONCLUSIONS

The approach proposed in this work shows how to improve a classic control system dedicated to VTOL operations over a moving target. In particular its shown that the trajectory tracking error might be improved and the UAS is able to perform a smooth VTOL manoeuvre over the USV.

The stability and softness provided by the dynamic movement primitives might be able to improve navigation manoeuvres subject to waves or even with wind gusts, and including dynamic obstacle avoidance capabilities. In spite of the early characteristic of this experimentation, the preliminary results hint of a sizeable improvement once more characteristics of the DMP are introduced into the control architecture.

Better performance could be expected, especially when performing repetitive cyclic and rhythmical tasks, typical in UAS based sensing techniques.

ACKNOWLEDGMENTS

The research leading to these results has received funding from the RoboCity2030-III-CM project (Robótica aplicada a la mejora de la calidad de vida de los ciudadanos. fase III; S2013/MIT-2748), funded by Programas de Actividades I+D en la Comunidad de Madrid and cofunded by Structural Funds of the EU.

REFERENCES

Davidson, K. and Schiff, L. (1946). Turning and course keeping qualities of ships. *Transactions of SNAME*, 4:49.

Djapic, V., Prijic, C., and Bogartz, F. (2015). Autonomous takeoff landing of small uas from the usv. In *OCEANS 2015 - MTS/IEEE Washington*, pages 1–8.

Erginer, B. and Altug, E. (2007). Modeling and pd control of a quadrotor vtol vehicle. In *2007 IEEE Intelligent Vehicles Symposium*, pages 894–899.

Fossen, T. I. (2011). *Handbook of marine craft hydrodynamics and motion control*. John Wiley & Sons.

Gams, A., Ijspeert, A. J., Schaal, S., and Lenarčič, J. (2009). On-line learning and modulation of periodic movements with nonlinear dynamical systems. *Autonomous robots*, 27(1):3–23.

Herissé, B., Hamel, T., Mahony, R., and Russotto, F.-X. (2012). Landing a vtol unmanned aerial vehicle on a moving platform using optical flow. *IEEE Transactions on Robotics*, 28(1):77–89.

Ijspeert, A. J., Nakanishi, J., Hoffmann, H., Pastor, P., and Schaal, S. (2013). Dynamical movement primitives: learning attractor models for motor behaviors. *Neural computation*, 25(2):328–373.

Ijspeert, A. J., Nakanishi, J., and Schaal, S. (2003). Learning attractor landscapes for learning motor primitives. *Advances in neural information processing systems*, pages 1547–1554.

Nemec, B., Tamošiūnaitė, M., Wörgötter, F., and Ude, A. (2009). Task adaptation through exploration and action sequencing. In *Humanoid Robots, 2009. Humanoids 2009. 9th IEEE-RAS International Conference on*, pages 610–616. IEEE.

Omar, V. A. (2017). Modelling and control of a uav-usv collaboration scheme for fluvial operations. Bachelor's thesis, Univ. Carlos III de Madrid.

Ore, J.-P., Elbaum, S., Burgin, A., Zhao, B., and Detweiler, C. (2015). *Autonomous Aerial Water Sampling*, pages 137–151. Springer International Publishing, Cham.

Perez, T. and Blanke, M. (2002). *Mathematical ship modelling for control applications*. Ørsted-DTU, Automation.

Pinto, E., Santana, P., Marques, F., Mendonça, R., Lourenço, A., and Barata, J. (2014). On the design of a robotic system composed of an unmanned surface vehicle and a piggybacked vtol. In *Doctoral Conference on Computing, Electrical and Industrial Systems*, pages 193–200. Springer.

Schaal, S., Peters, J., Nakanishi, J., and Ijspeert, A. (2005). Learning movement primitives. In *Robotics Research. The Eleventh International Symposium*, pages 561–572. Springer.

Weaver, J. N., Frank, D. Z., Schwartz, E. M., and Arroyo, A. A. Uav performing autonomous landing on usv utilizing the robot operating system.